Supplementary Information for

Understanding xenon and vacancy behaviors in UO_2, UN and U_3Si_2: A comparative DFT+*U* study

Jiajun Zhao[1], Dan Sun[2], Liu Xi[1], Ping Chen[2], Jijun Zhao[1,3], Yuanyuan Wang[1,3*]

[1] *Key Laboratory of Materials Modification by Laser, Ion and Electron Beams (Ministry of Education), Dalian University of Technology, Dalian, Liaoning, China*

[2] *Science and Technology on Reactor System Design Technology Laboratory, Nuclear Power Institute of China, Chengdu, Sichuan, China*

[3] *State Key Laboratory of Structural Analysis, Optimization and CAE Software for Industrial Equipment, Dalian University of Technology, Dalian 116024, China*

Table S1 Effect of supercell size on the formation energies of V_U in both UO_2 and UN as well as $V_{U\text{-}2}$ in U_3Si_2. The cutoff energy of 500 eV with the *k*-point grid spacing of 0.04 Å^{-1}, 0.02 Å^{-1} and 0.03 Å^{-1} is used for UO_2, UN and U_3Si_2, respectively. The supercell sizes highlighted in bold are employed in current work.

UO_2		UN		U_3Si_2	
Supercell size	E_f (eV)	Supercell size	E_f (eV)	Supercell size	E_f (eV)
1 × 2 × 2	12.75	1 × 2 × 2	6.05	2 × 2 × 2	1.65
2 × 2 × 2	**11.60**	**2 × 2 × 2**	**5.35**	2 × 2 × 3	1.49
2 × 2 × 3	11.28	2 × 2 × 3	5.72	**2 × 2 × 4**	**1.51**
				2 × 2 × 5	1.76

* Corresponding author's e-mail: yuanyuanwang@dlut.edu.cn (Y.Y. Wang)

Table S2 Predicted formation energies (E_f) of different types of mono-atomic vacancies and mono-atomic interstitials in UO_2, UN and U_3Si_2 by comparing with the existing data.

		Standard reference	U-rich state	X-rich (X = O, N, Si) state
UO_2	V_U	10.51	10.51	2.84
	Ref.	6.0 [1]	4.48 [2]	−6.50 [2]
	V_O	4.71	−0.91	2.93
	Ref.	5.6 [1]	−0.43 [2]	5.06 [2]
	U_i	2.59	2.59	10.26
	Ref.	8.2 [1]	2.50 [2]	13.48 [2]
	O_i	−0.34	5.28	1.44
	Ref.	−1.6 [1]	3.05 [2]	−2.44 [2]
UN	V_U	5.35	5.35	3.88
	Ref.	3.74 [3]; 6.90 [4]	3.66 [5]	2.09 [5]
	V_N	3.33	0.35	1.82
	Ref.	4.24 [3]; 7.91 [4]	0.62 [5]	1.42 [5]
	U_i	4.28	4.28	5.75
	Ref.	12.62 [4]	6.20 [5]	7.77 [5]
	N_i	0.39	3.37	1.90
	Ref.	4.54 [4]	3.82 [5]	3.01 [5]
U_3Si_2	V_{U-1}	2.68	2.55	3.50
	Ref.	2.65 [6]; 3.00 [7]	3.00 [7]	2.96 [7]
	V_{U-2}	1.51	1.38	1.36
	Ref.	1.64 [6]; 1.69 [7]	1.69 [7]	1.65 [7]
	V_{Si}	1.56	0.89	0.92
	Ref.	2.48 [6]; 1.79 [7]	1.77 [7]	1.84 [7]
	U_i	2.30	2.43	2.45
	Ref.	1.66 [6]; 0.65 [6], 1.17 [6]; 0.87 [7]	0.86 [7]	0.91 [7]
	Si_i	0.14	0.80	0.77
	Ref.	0.10 [6]; 0.85 [6], −0.20 [6]; 0.55 [7]	0.57 [7]	0.50 [7]

Table S3 Incorporation energies (E_i) between Xe atom and the typical trap sites in UO_2, UN and U_3Si_2 by comparing with other DFT-calculated results.

		Our work	Ref.
UO_2	IS	9.45	11.11 [8]; 9.48 [9]
	V_U	2.85	2.5 [8]; 3.84 [9]; 5.18 [2]
	V_O	8.80	9.5 [8]; 6.89 [9]; 9.01 [2]
	$\{V_U : V_O\}$	1.89	2.45 [8]
	$\{V_U : 2V_O\}$	1.09	1.38 [8]; 1.18 [9]; 2.90 [2]
UN	IS	14.64	14.62 [10]; 14.64 [11]
	V_U	4.03	3.59 [10]; 4.50 [12]; 3.74 [11]
	V_N	8.87	8.6 [10]; 8.28 [12]; 8.45 [11]
	$\{V_U : V_N\}$	2.72 (in [100] direction), 4.08 (in [111] direction)	2.79 [11]; 3.37 (in [100] direction) [12]; 4.90 (in [111] direction) [12]
U_3Si_2	IS	3.86	6.07 [6]; 5.36 [7]
	$V_{U\text{-}1}$	0.17	3.39 [6]; 3.14 [7]
	$V_{U\text{-}2}$	0.01	3.15 [6]; 3.24 [7]
	V_{Si}	0.27	3.39 [6]; 3.26 [7]

Supplementary Note 1: Chemical potential range

With the experimental formation enthalpy of UO_2 (−11.25 eV [13, 14]), the chemical potential variation of U and O is restricted in a range of −11.25 eV < $\Delta\mu_U^{UO_2}$ < 0 eV and −5.63 eV < $\Delta\mu_O^{UO_2}$ < 0 eV, respectively. Further, more experimental formation enthalpies of binary U-O phase [14], including UO_2, U_4O_9, U_3O_8 and UO_3, are involved to assess the variation range of $\Delta\mu_U^{UO_2}$ and $\Delta\mu_O^{UO_2}$, which can be expressed as

$$-7.67\ \text{eV} < \Delta\mu_U^{UO_2} \quad 0 \tag{s1}$$

$$-5.62\ \text{eV} < \Delta\mu_O^{UO_2} \quad -1.78\ \text{eV} \tag{s2}$$

It should be pointed out that the chemical potential values of −1.78 eV and −7.67 eV are related to the critical points of intersection between UO_2 and U_4O_9 (i.e., $UO_{2.25}$) lines as shown in the $\Delta\mu_U^{UO_2}$ - $\Delta\mu_O^{UO_2}$ diagram (see Fig. S1(a)).

However, there is no available experimental data for the formation enthalpies of hyper-stoichiometric phases in binary U-O, U-N and U-Si phase diagram. The DFT-calculated total energies of uranium compounds are subsequently considered to obtain the U-rich boundary of chemical potentials [15]. All the used U-O and U-N phases in the first-principles calculations are performed using the same value of U_{eff} for the stoichiometric UO_2 and UN. The DFT-calculated μ_O as a function of μ_U in the U-O system are displayed in Fig. S1(b). It is found that the phase transition from UO_3 to U_2O_5, UO_2 and UO can occur by adding more U atoms. The DFT-calculated chemical potentials are shown as follows:

$$-9.77\ \text{eV} < \Delta\mu_U^{UO_2} \quad -1.19\ \text{eV} \tag{s3}$$

$$-5.54\ \text{eV} < \Delta\mu_O^{UO_2} \quad -1.25\ \text{eV} \tag{s4}$$

which can be fitted as $\Delta H_{UO_k}^{GGA+U} - \Delta H_{UO_k}^{Exp.} = -0.002k - 0.024$ according to the dispersed points in Fig. S2(a). The corrected range of chemical potential of UO_2 is limited by the critical points of intersection among the chemical potential lines of UO_2, U_2O_5 and UO in Fig. S1(c), which can be expressed as

$$-11.07\ \text{eV} < \Delta\mu_U^{UO_2} \quad -0.90\ \text{eV} \tag{s5}$$

$$-5.80\ \text{eV} < \Delta\mu_O^{UO_2} \quad -0.71\ \text{eV} \tag{s6}$$

From a comparison of chemical potential ranges, the difference assessed by experimental μ_U and μ_O values in Fig. S1(a) is smaller than that by the corrected

ones in Fig. S1(c). Additionally, a large deviation between the dispersed points and the fitting line is presented in Fig. S2(a). As a result, the experimental formation energy derived chemical potential is used as a consequence for UO_2, and the variation ranges of $\mu_U^{UO_2}$ and $\mu_O^{UO_2}$ are separately determined as follows:

$$-14.54\ \text{eV} < \mu_U^{UO_2} - 6.87\ \text{eV} \quad \text{(s7)}$$

$$-10.55\ \text{eV} < \mu_O^{UO_2} - 6.71\ \text{eV} \quad \text{(s8)}$$

Here, the values of $\mu_U^{UO_2}$ and $\mu_O^{UO_2}$ in U-rich UO_2 are equal to −6.87 eV and −10.55 eV, respectively. While for the O-rich condition, the values of $\mu_U^{UO_2}$ and $\mu_O^{UO_2}$ are calculated as −14.54 eV and −6.71 eV, respectively. The same approach in estimating chemical potential using experimental formation enthalpies [16-18] is applied for UN to assess the variation range of μ_U^{UN} and μ_N^{UN} as follows:

$$-8.34\ \text{eV} < \mu_U^{UN} - 6.87\ \text{eV} \quad \text{(s9)}$$

$$-11.28\ \text{eV} < \mu_N^{UN} - 9.81\ \text{eV} \quad \text{(s10)}$$

It is worthy to note that the values of μ_U^{UN} and μ_N^{UN} for U-rich UN are −6.87 eV and −11.28 eV, respectively, and in the case of N-rich UN, the values of μ_U^{UN} and μ_N^{UN} equal to be −8.34 eV and −9.81 eV, respectively. A comparison of experimentally measured, DFT-calculated and corrected chemical potentials of UN shown in Figs. S2(d)-(f) indicates that the ranges of corrected μ_U^{UN} and μ_N^{UN} are much close to those of the experimentally measured ones. Therefore, the experimentally measured chemical potentials of U and N are employed in current work.

As for the chemical potential of hyper-stoichiometric U_3Si_2, the U-rich U_3Si_2 in equilibrium with γ-U_3Si and the Si-rich U_3Si_2 in equilibrium with U_3Si_5 are taken into account. By referring to the experimental formation enthalpies of U_xSi_y [15], the ferromagnetism property and U_{eff} = 1.0 eV are used in the formation enthalpy calculation of U_xSi_y. The variation ranges of corrected chemical potentials $\mu_U^{U_3Si_2}$ and $\mu_{Si}^{U_3Si_2}$ are predicted as follows:

$$-7.02\ \text{eV} < \mu_U^{U_3Si_2} - 7.00\ \text{eV} \quad \text{(s11)}$$

$$-6.08\ \text{eV} < \mu_{Si}^{U_3Si_2} - 6.05\ \text{eV} \quad \text{(s12)}$$

In the case of U-rich U_3Si_2, $\mu_U^{U_3Si_2} = -7.00$ eV and $\mu_{Si}^{U_3Si_2} = -6.08$ eV are separately obtained, and for Si-rich U_3Si_2, $\mu_U^{U_3Si_2} = -7.02$ eV and $\mu_{Si}^{U_3Si_2} = -6.05$ eV are identified, respectively. In Figs. 2(g)-(i), it is obviously found that the variation in $\mu_U^{U_3Si_2}$ and $\mu_{Si}^{U_3Si_2}$ are nearly the same as those of the DFT-calculated ones. The corrected GGA+*U* approximation could evidently reduce the range of chemical potential in U_3Si_2. Hence the corrected chemical potentials of U and Si are applied. As is known, the phases in binary U-Si phase diagram are really complex for DFT calculations, and more formation enthalpies of U_xSi_y species should be experimentally measured in the future.

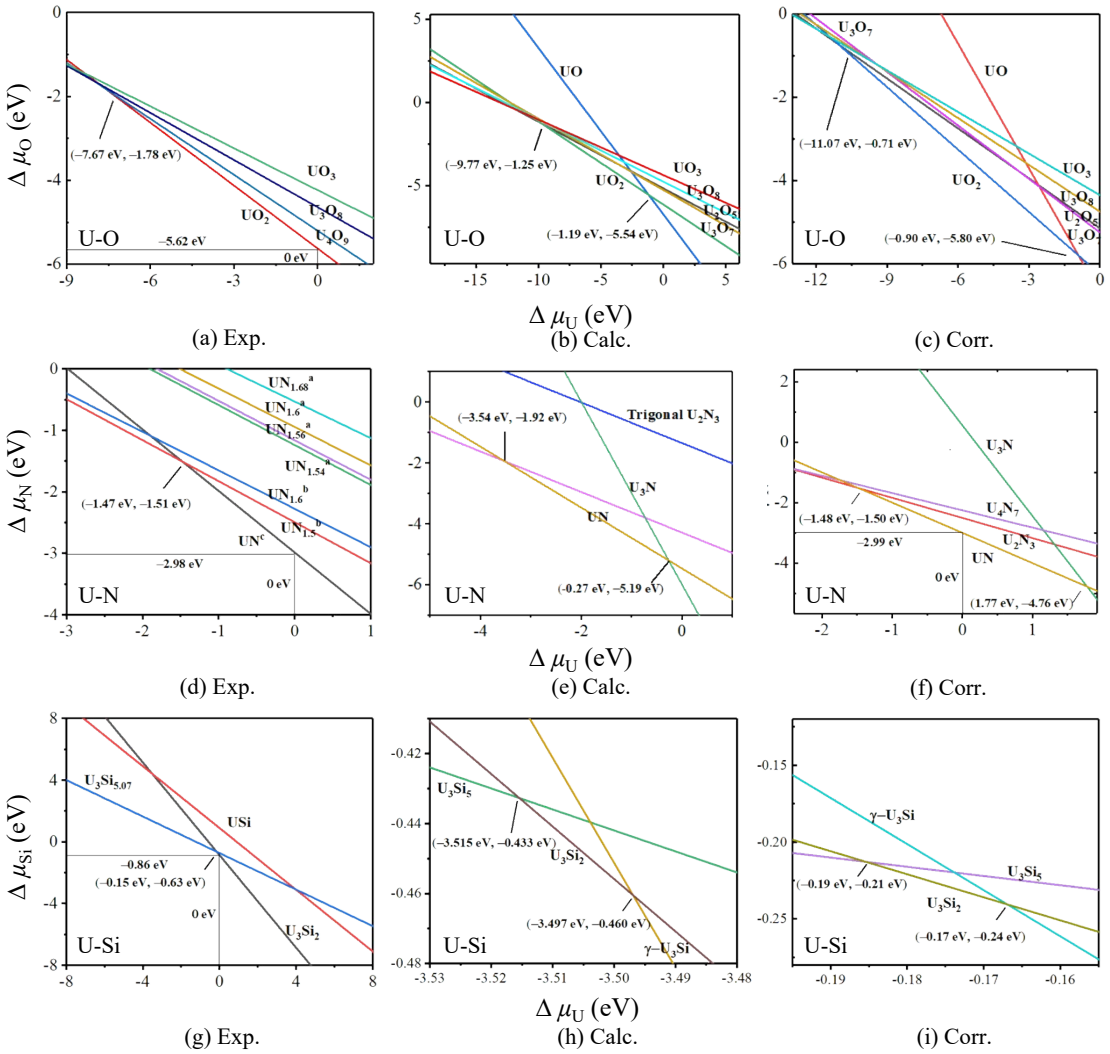

Fig. S1 (a)-(c) $\Delta\mu_O$ of the U-O phases, (d)-(f) $\Delta\mu_N$ of the U-N phases and (g)-(i) $\Delta\mu_{Si}$ of the U-Si phases as a function of $\Delta\mu_U$. The formation enthalpies are evaluated using (a)(d)(g) the experimental data, (b)(e)(h) the DFT-calculated data and (c)(f)(i) the data corrected from the Jain's approach. The superscript [a, b, c] respectively indicate the results from the work of Katsura and Serizawa [16], Katsura and Sano [17], and Hiroaki [18].

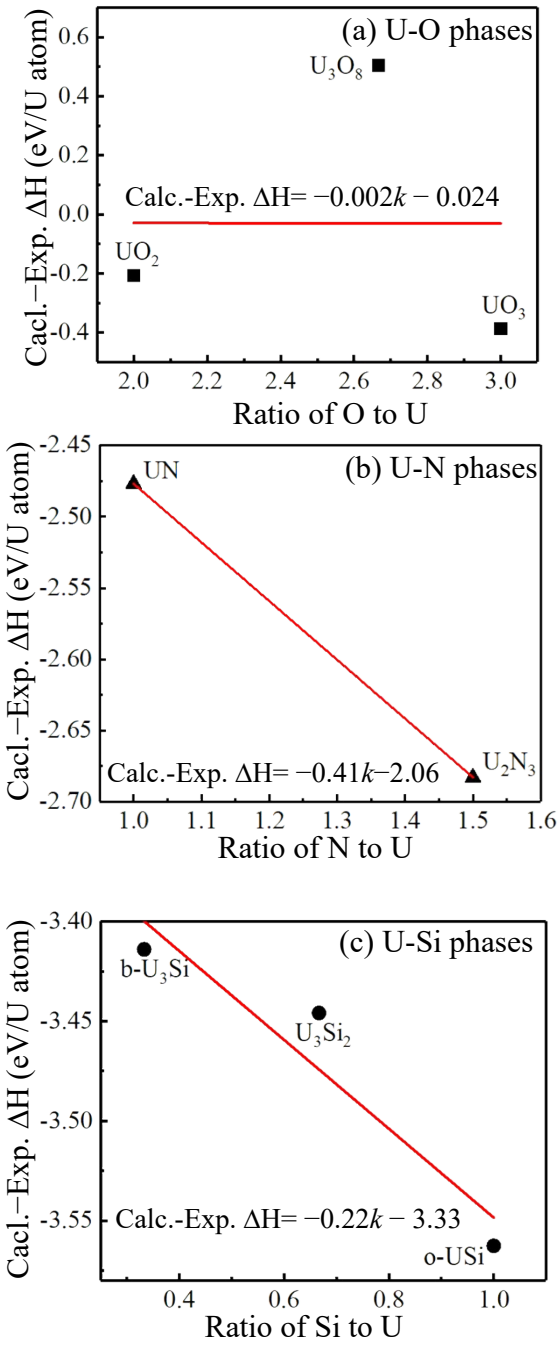

Fig. S2 Difference between the calculated and experimental formation enthalpies as a function of the ratio of X (X = O, N, Si) to U in (a) UO_2, (b) UN and (c) U_3Si_2. The red lines are fitted via least-squares to the binary U-O, U-N and U-Si systems, respectively. *k* represents the ratio of X atom number to U atom number.

Supplementary Note 2: Verification of formation energies

Most of the formation energy values of point defects in UO_2, UN and U_3Si_2 agree well with the reference ones. In the standard reference, the formation energy values of defects in UO_2 are ordered as: $V_U > V_O > U_i > O_i$, while Gupta et al. [1] found that the formation energy of mono-interstitial U is the highest one among the investigated point defects (i.e., $U_i > V_U > V_O > O_i$). In the U-rich environment of UO_2, the predicted and other DFT-calculated values of formation energy decrease in the order of $V_U > O_i > U_i > V_O$ [2], and our energetic trend of $U_i > V_U > O_i > V_O$ in O-rich UO_2 confirms well with that in Ref. [2].

As for UN in the standard reference, the order of current formation energies of V_U, V_N, U_i and N_i change to $V_U > U_i > V_N > N_i$, which substantially differs from those of $U_i > V_N > V_U > N_i$ [4]. Such different orders of V_U and U_i in not only UO_2 but also UN come from different choice of U_{eff} for α-U. A slight difference in the E_f order of U-rich UN between our result (i.e., $V_U > U_i > N_i > V_N$) and other DFT-calculated data (i.e., $U_i > V_U > N_i > V_N$ [5]) originates from the fact that our experimental data corrected chemical potentials shown in Fig. S1(i) are lower than the DFT derived ones used in Ref. [5]. Meanwhile, the values of E_f in the N-rich case are in the order of $U_i > V_U > N_i > V_N$, in accordance with the overall trend predicted by Kocevski et al. [5].

Comparing the results of U_3Si_2 under the standard reference with those in Refs. [6] and [7], the evolution trend matches well with each other in the E_f^V order of $V_{U\text{-}1} > V_{Si} > V_{U\text{–}2}$ and the E_f^i order of $U_i > Si_i$. It should note that our interstitial U (U_i) inserted at the U octahedron site (i.e., 2b site [19, 20]) remains in the octahedral site after relaxation. The formation energies of mono-vacancy and mono-interstitial U and Si are ordered as $V_{U\text{-}1} > V_{U\text{–}2} > V_{Si}$ and $U_i > Si_i$, respectively, in not only U-rich but also Si-rich U_3Si_2 samples, which slightly deviate from the prediction [7]. It can be explained by different magnetic considerations in these work.

Reference

1. F. Gupta, G. Brillant and A. Pasturel, *Philos. Mag.*, 2007, **87**, 2561-2569.
2. J. Yu, R. Devanathan and W. J. Weber, *J. Phys-Condens. Mat.*, 2009, **21**, 435401.
3. M. Klipfel and P. Van Uffelen, *J. Nucl. Mater.*, 2012, **422**, 137-142.
4. J. H. Lan, Z. C. Zhao, Q. Wu and Y. L. Zhao, *J. Appl. Phys.*, 2013, **114**, 202.
5. V. Kocevski, D. A. Rehn, M. W. D. Cooper and D. A. Andersson, *J. Nucl. Mater.*, 2021, **22**, 153401.

6. A. D. Andersson, *Density functional theory calculations of defect and fission gas properties in U-Si fuels*, United States, 2016.
7. D. A. Andersson, X. Y. Liu, B. Beeler, S. C. Middleburgh, A. Claisse and C. R. Stanek, *J. Nucl. Mater.*, 2019, **515**, 312-325.
8. P. V. Nerikar, X. Y. Liu, B. P. Uberuaga, C. R. Stanek and S. B. Sinnott, *J. Phys-Condens. Mat.*, 2009, **21**, 435602.
9. P. Garcia, G. Martin, C. Sabathier, G. Carlot, A. Michel, P. Martin, B. Dorado, M. Freyss, M. Bertolus and R. Skorek, *Nucl. Instrum. Meth.*, 2012, **277**, 98-108.
10. A. Claisse, T. Schuler, D. A. Lopes and P. Olsson, *Phys. Rev. B*, 2016, **94**, 174302.
11. A. Claisse, M. Klipfel, N. Lindbom, M. Freyss and P. Olsson, *J. Nucl. Mater.*, 2016, **478**, 119-124.
12. M. Klipfel, V. Di Marcello, A. Schubert, J. van de Laar and P. Van Uffelen, *J. Nucl. Mater.*, 2013, **442**, 253-261.
13. C. Guéneau, M. Baichi, D. Labroche, C. Chatillon and B. Sundman, *J. Nucl. Mater.*, 2002, **304**, 161-175.
14. Emerson, Vathonne, Julia, Wiktor, Michel, Freyss, Gérald, Jomard, Marjorie and Bertolus, *J. Phys-Condens. Mat.*, 2014, **26**, 325501.
15. C.-K. Chung, X. Guo, G. Wang, T. L. Wilson, J. T. White, A. T. Nelson, A. Shelyug, H. Boukhalfa, P. Yang, E. R. Batista, A. A. Migdisov, R. C. Roback, A. Navrotsky and H. Xu, *J. Nucl. Mater.*, 2019, **523**, 101-110.
16. M. Katsura and H. Serizawa, *J. Alloy. Compd.*, 1992, **187**, 389-399.
17. Masahiro KATSURA and T. SANO, *J. Nucl. Sci. Technol.*, 1967, **4**, 283-288.
18. T. Hiroaki, *J. Nucl. Mater.*, 1974, **51**, 78-89.
19. V. Kocevski, D. A. Lopes, A. J. Claisse and T. M. Besmann, *Nat. Commun.*, 2020, **11**, 2621.
20. S. C. Middleburgh, A. Claisse, D. A. Andersson, R. W. Grimes, P. Olsson and S. Mašková, *J. Nucl. Mater.*, 2018, **501**, 234-237.